

# RSC Advances



This is an *Accepted Manuscript*, which has been through the Royal Society of Chemistry peer review process and has been accepted for publication.

*Accepted Manuscripts* are published online shortly after acceptance, before technical editing, formatting and proof reading. Using this free service, authors can make their results available to the community, in citable form, before we publish the edited article. This *Accepted Manuscript* will be replaced by the edited, formatted and paginated article as soon as this is available.

You can find more information about *Accepted Manuscripts* in the [Information for Authors](#).

Please note that technical editing may introduce minor changes to the text and/or graphics, which may alter content. The journal's standard [Terms & Conditions](#) and the [Ethical guidelines](#) still apply. In no event shall the Royal Society of Chemistry be held responsible for any errors or omissions in this *Accepted Manuscript* or any consequences arising from the use of any information it contains.

# Synthesis of zirconium oxycarbide powders using Metal-Organic Framework (MOF) compounds as precursors

Jérémy David<sup>†,‡</sup>, Gilles Troliard<sup>†</sup>, Christophe Volkringer<sup>§</sup>, Thierry Loiseau<sup>§</sup> and Alexandre Maître<sup>†</sup>

<sup>†</sup> : SPCTS-CNRS, UMR 7315, Centre Européen de la Céramique (CEC), 12 Rue Atlantis - 87068 Limoges Cedex, France

<sup>‡</sup> : Present address: Center for Nanotechnology Innovation@NEST Istituto Italiano di Tecnologia, Piazza San Silvestro 12, 56127 Pisa, Italy

<sup>§</sup> : Unité de Catalyse et Chimie du Solide (UCCS) UMR CNRS 8181, Université de Lille, Sciences et Technologies, Avenue Mendeleïev, Bâtiment C7, BP 90108 - 59652 Villeneuve d'Ascq Cedex, France.

## **Keywords:**

Zirconium (oxy) carbide, Synthesis, Metal-Organic Frameworks, Electron microscopy.

---

Author to whom the correspondence should be addressed.  
Tel.:  
E-mail:

Gilles Troliard  
+ 33 587 502 381  
[gilles.troliard@unilim.fr](mailto:gilles.troliard@unilim.fr)

**Abstract:**

ZrC<sub>x</sub>O<sub>y</sub> oxycarbides were synthesized for the first time by using Metal-Organic Framework (MOF) compounds as precursors. These MOFs, based on zirconium carboxylates, are derived from the UiO-66 type structure. Three different Zr-MOF compounds were synthesized, differing by their C/Zr ratio, due to the use of terephthalic acid (C/Zr=8, or UiO-66), naphthalene-2,6-dicarboxylic acid (C/Zr=12) and biphenyl-4,4'-dicarboxylic acid (C/Zr=14 or UiO-67). The oxycarbides crystallites obtained through appropriate thermal treatments (under Ar atmosphere) of the Zr-MOF precursors show an average size of few hundred microns. They are surrounded by an outer rim of turbostratic carbon, which thickness is directly relevant to the C/Zr ratio coming from the nature of the organic linker. The composition of the oxycarbides obtained was estimated on the basis of the cell parameters refined from the powder XRD patterns. The oxycarbides synthesized from naphthalene-2,6-dicarboxylic acid and biphenyl-4,4'-dicarboxylic acid are close to ZrC<sub>0.925</sub>O<sub>0.075</sub>, while that of the oxycarbide obtained from terephthalic acid precursor is ZrC<sub>0.944</sub>O<sub>0.056</sub>. It results that the carbon richer oxycarbide product is observed for the UiO-66 precursor synthesized with terephthalic acid, and exhibiting the lower C/Zr ratio of the series. The composition of the oxycarbide powders is shown to be directly relevant to the mechanisms of decomposition of the Zr-MOF compound involved during heating.

## Introduction

Ultra refractory carbides are really suitable for ultra-high temperature applications thanks to their high properties, high hardness, good wear resistance and high decomposition temperature. In particular, because of its neutronic transparency, the zirconium carbide is being considered for application in Generation IV reactors, for example as barriers retaining the fission products in nuclear reactors. In this context, the reproducible fabrication of carbide or oxycarbide-based ceramics with well-controlled microstructure (*e.g.* grain size density) by hot pressing requires a high controlled quality of the starting powders, which must present a perfectly defined crystal size and a homogeneous chemical composition at different scale.

The carbothermal reduction of metal oxide by carbon black is the most conventional way to produce low cost oxycarbide powders in large amount with good reproducibility [1-3]. Other methods of synthesis such as sol-gel [4-6] or polymer-derived ceramic [7] routes are not really promising although they provide to nano-sized carbide particles with a near-stoichiometric composition and low oxygen content. Unfortunately, these latter routes provide obvious agglomeration which lead to heterogeneous microstructure after sintering due to their different sinterability. In the same manner, the self-propagating high-temperature synthesis (SHS) can be studied to produce ultrafine zirconium carbide powders [8-9] since low temperatures of ignition and low heat treatment durations are usually required. Nevertheless, owing to the rapidness and unstable propagation of the combustion wave front, the reaction information involved in SHS process still keeps poorly understood. Consequently, the manufacturing of nanosized zirconium carbide particles showing well-controlled chemical composition remains uncertain.

The reaction mechanisms involved in the production of zirconium oxycarbide powders by the carboreduction of oxides induce a composition distribution in the final product. It usually occurs at the early stage of the oxycarbide formation [10], due to the initial heterogeneous mixture (carbon black and metal oxide) at microscopic scale. Nevertheless, chemical homogenization of the starting powdered reactants is conceivable, but requires long annealing treatment, giving rise invariably to grain growth process. The fabrication of

oxycarbide nanopowders with grain size lower than 10-20 nm is then impossible by using this route.

During carbothermal reaction, it has also been shown that the initial grain size of the starting metal oxide powders may influence the carbide grain size as well as the structural type of added carbon [11]. Few attempts were also carried out to get a more uniform dispersion of carbon by mixing it under different chemical and structural forms [7, 12-14]. But this method did not lead to the formation of the desired strictly nanometer scale particles of metal carbides.

In this paper, we propose a new route for the production of zirconium oxycarbides by using Metal-Organic Framework-like compounds, bearing zirconium metallic centres together with carboxylic acid ligands (Zr-MOF) as precursors [15]. In these compounds, zirconium and carbon are intrinsically associated via direct Zr-O-C bondings, which give rise to the generation of three-dimensional open networks delimiting cavities. By using dicarboxylate linkers, the well-known compounds of the UiO-66 [15] series can be isolated. The frameworks have general formula  $\{Zr_6O_4(OH)_4(L)_6\}$  (L = ligand dicarboxylate:  $O_2C-(C)_n-CO_2$ ) and exhibit ccf packing of  $Zr_6O_4(OH)_4$  poly-oxo/hydroxo sub-units, in which zirconium is eight-fold coordinated in a square base  $[ZrO_8]$  antiprism. These hexanuclear bricks are interconnected through ditopic ligands with different lengths, related to the number of carbon of the aliphatic or aromatic part separating the carboxylate groups. Owing to their open structures, these microporous materials have promising applications in the fields of hydrogen [15-16], methane or carbon dioxide [17-25], alkane storage [26-27], and catalysis [28].

Nevertheless, these hybrid organic-inorganic compounds could also be good candidates as precursors to get oxides and oxycarbides after subsequent thermal treatments. Up to now, the pyrolysis of MOF-type compounds was currently investigated in order to create nanoporous carbon materials. In this context, the inherent porosity of the MOF structure induces a role of template for preparing such porous carbons [30-31]. In such studies, the MOF compound is calcined at high temperature ( $> 900^\circ\text{C}$ ) under inert atmosphere in the presence of furfuryl alcohol, which is previously polymerized within the

pore system at 150°C. Zinc-based MOF have been tested for such experiments since the ZnO phase obtained at 800°C is reduced during the carbothermal process and vaporized Zn metal is evacuated along with the gas flow. The resulting product is a purely porous hierarchical carbon, free of metal or oxygen. Following this strategy, porous carbon materials have been obtained directly without adding any carbon source, by varying the Zn/C ratio, coming from the intrinsic MOF composition, or the structure types [32-35]. Other works described the formation of porous carbon from Al-based MOF precursors, with the elimination of the resulting Al<sub>2</sub>O<sub>3</sub> solids by HF treatment [36].

In this contribution, we used different zirconium dicarboxylates derived from the UiO-66 topology and studied their thermal decomposition under inert atmosphere in a graphite furnace, with the aim to generate zirconium oxycarbides (ZrC<sub>x</sub>O<sub>y</sub>). In the studied chemical systems, the occurrence of direct Zr-O-C bonding in the precursor's structure may lower the diffusion length of carbon involved in the process of the formation of oxycarbides, compared to the carbothermal reduction route based on the reaction of zirconia and carbon black. In the case of MOF's, faster reaction kinetics are then expected. This would produce oxycarbide powders at lower temperature with limited duration of the annealing time, which would give rise to the nano-sized carbide materials.

The Zr-C-O system is also interesting because the ZrC<sub>x</sub>O<sub>y</sub> oxycarbides show a large range of solid solution [10, 37] that extended between ZrC<sub>0.95</sub>O<sub>0.05</sub> and ZrC<sub>0.70</sub>O<sub>0.30</sub>. It then seems interesting to check the influence of the chemical composition of the starting MOF precursor (C/Zr ratio) on the composition of the obtained oxycarbides. The number of carbon atoms from the organic linker has been varied from C/Zr = 8 up to C/Zr = 14, when starting with terephthalic acid (C/Zr = 8; called UiO-66, [15]), naphthalene-2,6-dicarboxylic acid (C/Zr = 12) or biphenyl-4,4'-dicarboxylic acid (C/Zr = 14; called UiO-67, [15]) as organic ligands for the formation of the UiO-66-like compounds [15, 38-40]. Then, the variation of the carbon content of the starting organic-inorganic precursor (C/Zr) was explored in relation with the *final* ZrC<sub>x</sub>O<sub>y</sub> stoichiometry, since the O/Zr ratio remains constant (O/Zr = 5.33) in the UiO-66

series. The Zr-O-C chemical system has attracted our attention because the valence of zirconium regarding to the oxygen is well defined (compared to Ti).

In this work, the nanostructured oxycarbide powders were characterized by a coupled X-Ray Diffraction (XRD) and Transmission Electron Microscopy (TEM) approach and the nature of their nanostructure discussed in regard with the structural characteristics of the used precursors.

### I - Synthesis and characterization of UiO-66-like precursors

The synthesis of the precursors is derived from the solvothermal process used by Lillerud and co-workers in 2008 [15]. The general reaction accounting for the formation of MOF is as follows:



Zirconium tetrachloride (Sigma Aldrich, 99.99 %) and organic ligands such as carboxylic diacids (terephthalic acid, Sigma-Aldrich, 98 %, noted H<sub>2</sub>BDC; naphthalene-2,6-dicarboxylic acid, Sigma-Aldrich, 99 %, noted H<sub>2</sub>NDC; biphenyl-4,4'-dicarboxylic acid, Sigma-Aldrich, 97 %, noted H<sub>2</sub>PBDC) are mixed in a Teflon cell (vol. nearly 23 mL) in the presence of N,N-dimethylformamide (noted DMF: Sigma-Aldrich, anhydrous 99.8 %) as solvent. The different mixtures are then placed in a stainless steel Parr type autoclave and heated in an oven at 120°C during 24h. The autoclave was taken out of the oven and placed at room temperature to stop the solvothermal reaction. The obtained products are washed with DMF and then dried on a filter paper at room temperature under ambient condition. The resulting white powder obtained is then dried in an oven at 200°C, in order to remove solvent molecules encapsulated within the pores. The chemical reactants and some structural features of the UiO-66 like precursors are summarized in Table 1 based on data of [15, 36, 41].

*Zr-BDC compound* ( $\text{Zr}_6\text{O}_4(\text{OH})_4(\text{BDC})_6 \cdot x\text{DMF}$ ). It was obtained from the mixture of zirconium chloride and terephthalic acid in DMF solvent, with the following composition: ZrCl<sub>4</sub>: 88 mg, 0.38 mmol; H<sub>2</sub>BDC: 54.8 mg, 0.33 mmol; DMF: 4 mL. The resulting XRD

pattern (Figure 1a) is indexed with that of the Zr-BDC structure proposed by Cavka *et al.* [15]. A slight broadening of the diffraction lines is observed due to the small particles size. SEM observation shows that the product is formed of large aggregates of few microns size (Figure 1b), which are composed of crystals of few hundred nanometers size, showing cubic habit (Figure 1c) in agreement with the  $Fm\bar{3}m$  space group. Indeed, micro-twinned patterns are observed and correspond mainly to (111) twining law of interpenetrated crystals (Figure 1c). Energy dispersive spectrometry analysis confirms that chlorine remains trapped within crystals probably within the inner structural porosity (Figure 1d).

*Zr-NDC compound* ( $Zr_6O_4(OH)_4(NDC)_6 \cdot xDMF$ ). It was obtained from the mixture of zirconium chloride and naphthalene-2,6-dicarboxylic acid in DMF solvent, with the following composition:  $ZrCl_4$ : 83.5 mg, 0.36 mmol;  $H_2NDC$ : 76.7 mg, 0.35 mmol; DMF: 4 mL. The use of  $H_2NDC$  as a ligand has been recently reported to synthesise the UiO-66-like solids [38]. Compared to Zr-BDC, Zr-NDC sample is characterized by an XRD pattern showing both important line broadening reflecting small crystallites sizes and an intense background noise (Figure 2a). SEM observation confirms the occurrence of octahedral shaped crystallites (Figure 2 b-d) showing heterogeneous size distribution (from few tenths of nanometers to few hundred) embedded within powdered aggregates showing cauliflower morphology (Figure 2c). As demonstrated in a previous study [40], the occurrence of these aggregates is not assigned to impurities but is characteristic of the corresponding phase showing low crystallinity.

*Zr-BPDC compound* ( $Zr_6O_4(OH)_4(BPDC)_6 \cdot xDMF$ ). It was obtained from the mixture of zirconium chloride and biphenyl-4,4'-dicarboxylic acid in DMF solvent, with the following composition:  $ZrCl_4$ : 86.1 mg, 0.37 mmol;  $H_2PBDC$ : 83.8 mg, 0.35 mmol; DMF: 4 mL. The XRD pattern of Zr-BPDC is represented Figure 3a. As for Zr-NDC, a line broadening effect coupled with the presence of an intense background noise is observed. SEM images exhibit crystal assemblies displaying possible merohedral reticular twining patterns embedded in a pulverulent nano-crystallized matrix.

## II - Characterization techniques

After the filtering and drying step, the homogeneous white powdered samples have been characterized by XRD with the following acquisition conditions. X-ray diffraction intensities have been collected on a D8 apparatus (Bruker, Karlsruhe, Germany) within the angular range (2-theta) 5° - 50° (step: 0.195° - step time: 0.6 s), using  $K_{\alpha 1}$  /  $K_{\alpha 2}$  copper radiation.

The stoichiometry in carbon and oxygen of the oxycarbides was obtained by an indirect measurement of the cell parameters of the oxycarbide phase. This determination was possible thanks to a former work [37] in which we analysed the exact composition of different pure powder samples of oxycarbides that were synthesized to get a calibration curve of the composition versus the cell parameters owing to the Vegard law. During this study, the global analysis of oxygen and carbon content was achieved by elemental chemical analysis using combustion analysers: EMGA 600W (Horiba Kyoto Japan) for carbon and EMIA 221V (Horiba, Kyoto, Japan) for oxygen. These results were then comforted by X-ray Fluorescence measurements and electron microprobe analysis (CAMECA SX 100, Gennevilliers, France) using a  $ZrO_2$  and ZrC standards. This method requires an accurate determination of the cell parameter through careful treatment of the XRD patterns introducing a standard sample in order to correct data for sample positioning errors and get accurate cell parameters. The cell parameters were then determined using the Peakoc software [42], from the positions of the five first Bragg peaks, fitted with pseudo-Voigt functions. The error given by the software was multiplied by 3 to reach a satisfactory 99% confidence level.

A JEOL 7400 F (Cold Cathode) Scanning Electron Microscopy (SEM) operating at low voltage was used to observe the MOF-type compounds which are usually highly sensitive to the electron beam. The  $ZrC_xO_y$  oxycarbides were analysed by Transmission Electron Microscopy (TEM) by using a JEOL 2010 microscope (JEOL, Tokyo, Japan) operating at 200 kV. TEM samples were prepared by crushing the powders in an agate

mortar. Then they were put in suspension in a drop of water that was deposited on a copper grid covered by a holey carbon

### III - Formation and characterization of oxycarbides

Each Zr-MOF (UiO-66 type) sample was treated in a graphite furnace (V.A.S. furnace, Suresnes, France) under flowing argon ( $\sim 400 \text{ cm}^3 \cdot \text{min}^{-1}$ ) with the following procedure: a heating rate of  $20^\circ\text{C} \cdot \text{min}^{-1}$  until  $1750^\circ\text{C}$ , a hold at  $1750^\circ\text{C}$  for 8h before being cooling down to room temperature at  $20^\circ\text{C} \cdot \text{min}^{-1}$ . The thermal treatment is close to that usually used for conventional procedure (carbothermal reaction involving dioxide and carbon black [43]); even if the synthesis temperature of carbide is expected to be lower. In fact, these conditions were considered in order to optimize the probability to form a  $\text{ZrC}_x\text{O}_y$  oxycarbide and reach the final advancement degree (noted  $\xi_{\text{max}}$ ) of the reaction. In addition, this protocol will allow for comparing the two synthetic routes (conventional carbo-reduction and our work) of the  $\text{ZrC}_x\text{O}_y$  oxycarbides with a reproducible and standardized manner.

#### ***X-ray diffraction results obtained on the different oxycarbides powders.***

The XRD patterns of each of UiO-66 like compound precursors heated at  $1750^\circ\text{C}$  for 8h, are shown in figure 4. They are indexed in agreement with the JCPDS data file number 035-0784 corresponding to the cubic single-phase zirconium carbide. Compared to this carbide standard, the obtained carbides show a slight shift of the diffraction peaks towards the high angle  $2\theta$  values that correspond to a smaller metrics of the cell parameter. This behaviour may be relevant to a sub-stoichiometry in carbon ( $\text{ZrC}_{1-x}$ ) or the formation of an oxycarbide ( $\text{ZrC}_x\text{O}_y$ ). Indeed, previous studies [37, 43] have reported that the lattice parameter of the  $\text{ZrC}_x\text{O}_y$  phase is significantly modified by the incorporation of oxygen in the  $\text{ZrC}_x$  lattice that can be substituted to carbon. It was shown that the lattice parameter of samples decreases when increasing oxygen content since the radius of oxygen ( $R_{\text{O}} = 0.64 \text{ \AA}$ ) is lower than that of carbon ( $R_{\text{C}} = 0.77 \text{ \AA}$ ).

All the XRD patterns obtained on the three products display sharp diffraction peaks (Figure 4). In particular, the enlargements of the 511 diffraction peaks of the three patterns (see insets in Figure 4 and Figure 5) show that the two  $K_{\alpha_1}$  and  $K_{\alpha_2}$  diffraction lines due to the copper anticathode of the diffractometer are clearly separated. It is thus deduced that in these samples the crystal size must be important enough (> few microns) to avoid any broadening effect and that the crystals can be assumed at first glance to be free of defects together with well-defined composition. It is however to be noticed that if the Full Widths at Half Maximum (FWHM) values of the 511  $K_{\alpha_1}$  diffraction peaks are similar for ZrC-NDC and ZrC-BPDC (0.209° and 0.214° in  $2\theta$  angle respectively), it is significantly larger for ZrC-BDC (FWHM = 0.140° in  $2\theta$  for  $K_{\alpha_1}$ ). In the latter, the shaping profile of the diffraction peaks is very close to that of the instrumental function. Compared to ZrC-BDC, the carbide obtained from Zr-NDC precursor displays broader diffraction lines. They are probably due to a smaller grain size, internal microstrains or non-homogeneous composition of the carbide grains.

Figure 5 shows the superimposition of the 511 peaks of the three compounds. While 511 lines of oxycarbides obtained from NDC and BPDC are nearly localized on the same  $2\theta$  position, the 511 lines of the BDC oxycarbide are slightly shifted through the lower values of  $2\theta$ . The displacement of the diffraction peaks toward the low diffraction angles is relevant to a higher parameter value, related to higher carbon content. For ZrC-BDC, the cell parameter has been determined as  $a=4.69551 \pm 0.00003 \text{ \AA}$ . This value is slightly lower than that found in the purely stoichiometric carbide ( $a=4.697 \text{ \AA}$  according to the JCPDS data file), so that we can assume that this compound presents a chemical composition nearly saturated in carbon. In contrast, the cell parameters determined for the two other oxycarbides are respectively  $a=4.69295 \pm 0.00006 \text{ \AA}$  and  $a=4.69282 \pm 0.00006 \text{ \AA}$  for ZrC-NDC and ZrC-BPBC compounds. This lower parameter value seems to indicate an oxygen richer composition.

From the X-ray diffraction study, it is then concluded that higher C/Zr ratio leads to lower cell parameter for the resulting carbide. This apparent disagreement will be further on tackled in the discussion session.

Finally, in the ZrC-NDC sample, the XRD pattern also indicates the presence of a restricted amount of tetragonal zirconia (JCDPS data file n° 00-042-1164) readily identified by the most intense 101 diffraction peak (Figure 4b: see squared area). In addition to the low value of the cell parameter, the presence of zirconia suggests that the system is either under-saturated in carbon or incompletely transformed.

### ***Electron microscopy results obtained on the different oxycarbides powders.***

The most characteristic microstructural features were observed on the carbon rich ZrC-BPDC samples. The results will then be first presented for this system and the results obtained on the ZrC-BDC ZrC-NDC systems will be presented for comparison.

The SEM observations (Figure 6) carried out on ZrC-BPDC samples reveal the occurrence of crystals reaching few hundred of nanometers (encircled region in Figure 6b) embedded within a powdered matrix (see arrow in Figure 6b). The proportion of the crystallized phase being largely predominant, these observations are in perfect agreement with the narrowness of the line profiles observed in the XRD patterns (Figure 4 and 5). The same results were obtained by SEM on the two other studied systems (ZrC-BDC and ZrC-NDC).

TEM observations performed on ZrC-BPDC samples show that the powdered regions consist in wide areas of amorphous carbon containing smaller sized crystals of zirconium carbides (Figure 7a), which are identified from the selected area electron diffraction (SAED) patterns. The nucleation of carbides then appears in carbon areas. The energy dispersive spectrometry analysis performed on the carbide crystals confirms the presence of oxygen and the formation of oxycarbides (Figure 7b). This result agrees with the smaller value of the lattice parameter compared to the pure zirconium carbide. The smaller cell parameters of the carbides are then better relevant to the incorporation of oxygen within the crystal lattice ( $\text{ZrC}_x\text{O}_y$ ) than to the formation of sub-stoichiometric carbide ( $\text{ZrC}_{1-x}$ ). The biggest faceted oxycarbides crystallites (Figure 6 and 7c), identified from the SAED patterns (Figure 7d), are all surrounded by a continuous rim of carbon. In addition to the spots of the oxycarbide lattice

corresponding to the [010] zone axis, the SAED pattern (Figure 7d) shows supplementary spots. The two measured distances (3.45 Å and 2.09 Å: see arrows) are characteristics of the 2-dimensional character of the turbostratic carbon. Figure 7e shows that the growth of the carbon sheets is parallel to the crystalline faces of the carbide (Figure 7c). The orientation change between the crystalline faces is accommodated by kinks in the carbon layer. This result is confirmed by the analysis of the SAED patterns (Figure 7d) which shows that the [001]\* reciprocal rows of the turbostratic carbon are orientated normal to the crystalline faces of the oxycarbide grains. The presence of wedge fringes in the outer side of the crystals seems to indicate that the faces are not viewed edge on. In this case, {h0h} may solely be the projected trace of {111} type crystalline faces. The automorphous shape may then results from a lowering of the surface energy, probably due to the long-time of the annealing treatment at elevated temperature. Despite this harsh treatment, the presence of residual amorphous carbon seems to indicate that the carbon is in excess in the system. Two distinct carbon layers are observed. The inner layer, generally 15-20 nm thick, is well ordered (Figure 7e) even if a contrast fluctuation is observed, showing the presence of micro-strains probably due to the graphitization of the carbon layer (Figure 7f). The external layer is thinner (a few nanometers) and characterized by its amorphous character. The inner layer should have grown during the decomposition of the Zr-BPDC precursor and the external one may have appeared during further cooling of the sample.

TEM analysis of the powdered regions of the ZrC-BDC samples shows at first sight similar results (Figure 8). These regions are however composed of automorphous oxycarbide crystals appearing inside large areas of amorphous carbon (Figure 8b). Facets were clearly indexed by electron diffraction experiments (Figure 8 b-c) as being {111} and {100} type crystalline faces, i.e. the most dense planes of the structure. The oxycarbide crystals are surrounded by a double carbon layer. The much darker inner one corresponds to the turbostratic carbon (Figure 8d), as identified by elongated diffraction spots observed within the SAED patterns (Figure 8c). The average inter-reticular distance, close to 3.8 Å, is slightly greater than the expected value ( $\approx 3.4$  Å). Dispersive spectrometry analysis indicates the

intercalation of small amount of zirconium atoms in the carbon layers. This explains the strengthening of the diffraction spots observed in the SAED patterns and the darker Z-contrast observed. The global thickness of the carbon layer ranges from 3 to 5 nm. It is in any case much thinner than that encountered in the ZrC-BPDC system previously described (15-20 nm).

TEM observations performed on the ZrC-NDC system show that the oxycarbides crystals grow in amorphous carbon areas (Figure 9a). They present an average size of 200 nm (Figure 9b) in fair agreement with the line broadening observed in the XRD patterns (see Figures 4b and 5). Here, the crystallites are embedded within an external double layer of carbon with thickness values ranging from 7 to 12 nm. It is then concluded that the thickness of the external double layers of carbon is directly correlated to the initial C/Zr ratio of the starting system (Table 1). As in the ZrC-BDC system, the inner carbon layer is composed of turbostratic carbon showing darker contrast, which is probably related to the occurrence of intercalated compounds.

#### IV - Discussion

Whatever the MOF precursor, the formation of thick turbostratic carbon layer surrounding the oxycarbide particles may lead to an excess of carbon in the system, which may appear as graphite into ceramics monolith during the powders sintering. In a near future, additional attempts will be performed by using MOF precursors characterized with lower C/Zr ratio. Indeed, it is interesting to note that the thickness of the double layer: 15-20 nm for ZrC-BPDC, 7-12 nm for ZrC-NDC and 3-5 nm for ZrC-BDC is directly controlled by the C/Zr ratio prevailing within the MOF precursors, respectively 14, 12 and 8. The amount of carbon in the final carbide system can then be adjusted by the choice of the MOF precursor.

The inner layer of turbostratic carbon contains zirconium atoms and should have been formed during the zirconium carbide growth. The external amorphous carbon showing weaker contrast is zirconium free. It could appear lately during the cooling of the sample as

resulting from re-condensation of carbon monoxide that may emerge during the decomposition of the precursor during the heat treatment.

Each MOF precursor also exhibits a constant O/Zr ratio of 5.33, which leads to the formation of oxycarbide grains instead of pure carbides. The size of the crystals reaches few hundred of nanometers (ranging from 150 to 500 nm) and is in the same order of magnitude for the case of classical carbothermal synthesis route. A complete study of the mechanisms involved in the transformation of precursors into oxycarbides was performed and will be published in a forthcoming paper [44] in order to understand the reason why nanometer-sized crystals could not be obtained by this synthesis way. The oxycarbides grains always show automorphous habit with the formation of the denser planes of the carbide structure thanks to a reduction of the surface energy occurring during the thermal treatment.

TEM analysis of samples revealed that the thicker inner layer of turbostratic carbon surrounding the oxycarbide grains is orientated, so that carbon sheets are parallel to the crystalline faces of the crystals. This feature case is specific from this chemical system and has not been observed during classical carbothermal reduction of zirconia with carbon black. In contrast, for the latter procedure, the presence of an oxygen rich amorphous layer is usually observed around the oxycarbides at least during the earlier stage of the crystal growth. Its presence was attributed [43] to the co-condensation of  $ZrO_{(g)}$  and  $CO_{(g)}$  species which occurs during the oxycarbide formation. This reaction locally induces an excess of oxygen, which is slowly resorbed at the contact with the residual carbon black during the later step of the reaction. It is worth to be noted that such amorphous external layer rich in oxygen was never observed in the studied samples, even for the smallest oxycarbide grains. This result may be explained by the high original C/Zr ratios available within precursors as well as by the intimate proximity of carbon and zirconium within the MOF-type compounds.

Surprisingly, the two UiO-66 type precursors showing the higher C/Zr ratio gave rise to the formation of the less carbon rich oxycarbides. Figure 5 shows that both ZrC-BPDC and ZrC-NDC show very similar XRD pattern profiles with close  $2\theta$  positions indicating nearly equivalent chemical compositions. Based on the work of Gendre et al. [37], giving the

correlation between the value of the refined parameter and the C/O ratio for  $ZrC_xO_y$  oxycarbides, the estimated composition of these two oxycarbides are close to  $ZrC_{0.925}O_{0.075}$ , while that of the oxycarbide obtained from ZrC-BDC precursor, is  $ZrC_{0.944}O_{0.056}$ . It means that the oxycarbides could not get their equilibrium composition ( $ZrC_{0.980}O_{0.020}$ : see [31]) despite the harsh treatment procedure.

As the experimental conditions (temperature and dwelling time) are similar for the three syntheses, the different chemical compositions of the resulting products may be explained by the decomposition behaviour of each precursor during the thermal treatment. Their degradation mechanism depends on the bonding energy of, *i.e.* on the different natures of the ligands of the precursors. Figure 10 represents possible schemes of the decomposition of the three precursors, together with bonding ( $E_b$ ) and resonance ( $E_r$ ) energies (calculations based on Huckel theory). It is assumed that weaker energy bondings are first broken during the thermal treatment, since a two-step mechanism may be involved at least. For Zr-BDC (Fig. 10a), only two C-C bondings have to be first broken, followed by the degradation of the benzene group ( $E_{\text{resonance}} = 150.9 \text{ kJ.mol}^{-1}$ ). It seems that the energy provided by the thermal treatment is sufficient to release all the carbon required for the formation of the oxycarbide, which exhibits nearly stoichiometric composition close to ZrC. In comparison, it seems that more energy is needed to destabilize the organic part in both Zr-BPDC and Zr-NDC precursors. Indeed, Zr-BPDC precursor possesses three C-C bondings + two benzene groups that needed to be broken. In addition, the central C-C bonding may show a higher energy as being stabilized by the presence of the two neighbouring benzene groups and forming quite stable aromatic group ( $E_{\text{resonance}} = 294.3 \text{ kJ.mol}^{-1}$ ). The release of two benzene groups of the Zr-NDC precursor needs to break 2 C-C bondings. But owing to the presence of neighbouring two naphthalene groups ( $E_{\text{resonance}} = 256.7 \text{ kJ.mol}^{-1}$ ), their energy might be higher than that in the case of Zr-BDC precursor. In addition, after being released, the two benzene cycles of the naphthalene groups are connected through energetic double bondings

( $E_{\text{bonding}} = 602 \text{ kJ.mol}^{-1}$ ) difficult to be broken. Finally, both Zr-BPDC and Zr-NDC precursors are supposed to require higher decomposition energy than that for Zr-BDC. Thus, they could be only partially destabilized during the heating treatment. Then, longer reaction time or higher temperature is needed to achieve the precursor decomposition and to enrich correlatively the oxycarbide in carbon until its stoichiometric composition. This remark would explain why the resulting products obtained in the Zr-BPDC and Zr-NDC systems, contain larger oxygen amount related to shorter lattice parameters. The TEM observations indicate that the oxycarbides issued from the three precursors roughly present the same type of microstructures. Therefore, the enlargement of the diffraction peaks of the XRD patterns of Zr-NDC and Zr-BPDC is rather assigned to a heterogeneous chemical composition, suggesting that the thermodynamic equilibrium has not been reached in these samples, as well. This assumption of an incomplete reduction is also supported by the XRD results showing the presence of zirconia (Figure 4b: squared area) in the final product, which attests that the atmosphere is not sufficiently reductive during the heat treatment.

Finally, all the results reported above indicate that the Zr-BDC phase is the most adapted MOF-type precursor to generate carbon rich zirconium oxycarbides.

### Conclusions:

- 1) This study shows that MOF-like compounds can be used as precursors to synthesize oxycarbides, without adding any carbon black. This attempt is then promising even if the three studied chemical systems are saturated in carbon as shown by the occurrence of both residual amorphous carbon in samples and by the surrounding double layers of turbostratic carbon around the oxycarbide grains.
- 2) The thickness of the double carbon layer is directly controlled by the C/Zr ratio prevailing within the MOF precursors.
- 3) The estimated composition of the oxycarbides obtained from ZrC-BPDC and ZrC-NDC with respective C/Zr = 12 and 14 are close to  $\text{ZrC}_{0.925}\text{O}_{0.075}$ , while that of the oxycarbide obtained from ZrC-BDC precursor (C/Zr =8) is  $\text{ZrC}_{0.944}\text{O}_{0.056}$ . It is suggested that the amount

of carbon contained in the oxycarbides does not depend on the intrinsic carbon content of the ligands of MOFs but better rely on the carbon released during their decompositions, which is controlled by the bonding energies of the links involved in their structures.

4) Zr-BDC phase is the most adapted MOF-type precursor to generate carbon rich zirconium oxycarbides.

**Acknowledgements:**

The authors are thankful to P. Carles for his technical assistance for TEM applications. Gilles Trolliard is also grateful to Olivier Masson for his involvement in the interpretation of XRD data.

Table 1: Chemical reactants and structural features of the UiO-66 compounds

MOF Nomenclature	Chemical reactants				Structural Characteristics of the obtained precursors [15, 41, 36] respectively		Chemical characteristic of the precursors	
	Salt	Ligand	Ligand nomenclature	Solvent	Space Group	Cell parameter	C/Zr	O/Zr
Zr-BDC	ZrCl <sub>4</sub>	Terephthalic acid	H <sub>2</sub> BDC	DMF	<i>Fm</i> $\bar{3}m$	20.743 Å	8	5.33
Zr-NDC	ZrCl <sub>4</sub>	Naphthalene-2,6-dicarboxylic acid	H <sub>2</sub> NDC	DMF	<i>F</i> 23	23.785 Å	12	5.33
Zr-BPDC	ZrCl <sub>4</sub>	Biphenyl-4,4'-dicarboxylic acid	H <sub>2</sub> BPDC	DMF	<i>Fm</i> $\bar{3}m$	27.094 Å	14	5.33

## Figure captions

Figure 1: The MOF precursor obtained with terephthalic acid Zr-BDC (C/Zr=8)

- XRD patterns of a Zr-BDC powder.
- and c) SEM observations of the Zr-BDC sample showing agglomerates of few microns composed of elementary particles with grain size of 400-500nm.
- Energy dispersive spectrometry analysis of an individual grain of ZR-BDC.

Figure 2: The MOF precursor obtained with naphthalene-2,6-dicarboxylic acid Zr-NDC (C/Zr=12)

- XRD powder pattern of Zr-NDC.
- Low magnification SEM observations showing the presence of crystals (see arrows) together with agglomerates (encircled regions).
- Enlargement of agglomerate showing cauliflower type morphology.
- Enlargement of crystalline area showing the octahedral morphology of the Zr-NDC crystals.

Figure 3: The MOF precursor obtained with biphenyl-4,4'-dicarboxylic acid Zr-BPDC (C/Zr=14)

- XRD pattern of a Zr-BPDC powder.
- SEM overview of an aggregate of interpenetrated crystallites of Zr-BPDC.
- SEM micrograph showing the crystallites coexisting with pulverulent region that can be either micro-crystallized or amorphous area.

Figure 4: The XRD patterns obtained on the carbide powders.

- ZrC-BDC. An enlargement of the 511  $K_{\alpha 1}$  and  $K_{\alpha 2}$  peaks is provided as an insert.
- ZrC-NDC. An enlargement of the 511  $K_{\alpha 1}$  and  $K_{\alpha 2}$  peaks is provided as an insert.
- ZrC-BPDC. An enlargement of the 511  $K_{\alpha 1}$  and  $K_{\alpha 2}$  peaks is provided as an insert. In this diagram, the dome shaped area observed at the low Bragg angles (between 15 and 30°) is due to an artifact phenomenon related to the scattering of the underlying amorphous sample holder, since the thickness of the sample is very thin.

Figure 5: Representation of an enlarged region of the XRD patterns of the three powders of oxycarbides merging from the insets of figure 4.

Figure 6: SEM observations of a powder of ZrC-BPDC showing the heterogeneous microstructure of the sample composed of micron sized crystals embedded within a gangue.

Figure 7: TEM observations of the ZrC-BPDC sample.

- a) Overview.
- b) Low energy part of the energy dispersive spectrometry spectrum of a ZrC-BPDC particle attesting of the presence of oxygen.
- c) Gathering of ZrC-BPDC particles showing faceted morphologies. The presence of a continuous surrounding layer is evidenced.
- d) Selected area electron diffraction pattern of the particle on the right of c);
- e) Enlargement of the squared region of c) showing a carbon layer with its (001) planes parallel to the crystalline faces of the underlying crystal of oxycarbide.
- f) Carbon layer from another ZrC-BPDC particle showing the regular stacking of the carbon layers.

Figure 8: TEM observations of the ZrC-BDC sample.

- a) Overview.
- b) TEM observation of a ZrC-BDC and its superimposed corresponding electron diffraction pattern allowing the identification of the crystalline faces of the crystal viewed edge on. The white arrows point at the occurrence of streaked diffraction spots provided by the external layer of turbostratic carbon.
- c) Enlargement of the squared region of b) showing two carbon layers displaying contrasted changes due to a Z effect.

Figure 9: TEM observations of the ZrC-NDC sample.

- a) Overview.
- b) Regions showing nanometer sized crystals of ZrC-NDC are often observed.
- c) TEM observation of gathering of bigger ZrC-NDC particles.
- d) and e) Enlargements of carbon layers around ZrC-NDC particles showing the formation of a double layer of carbon, the inner one showing a darker contrast due to the incorporation of zirconium.

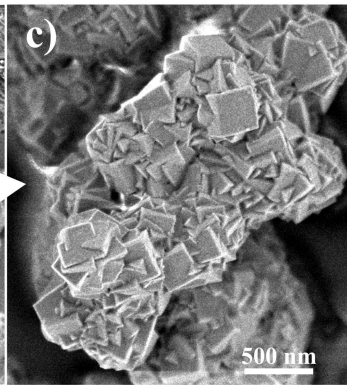
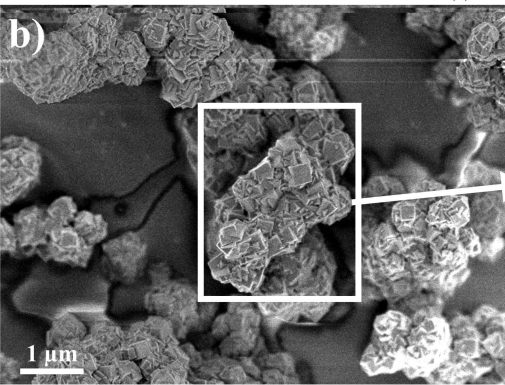
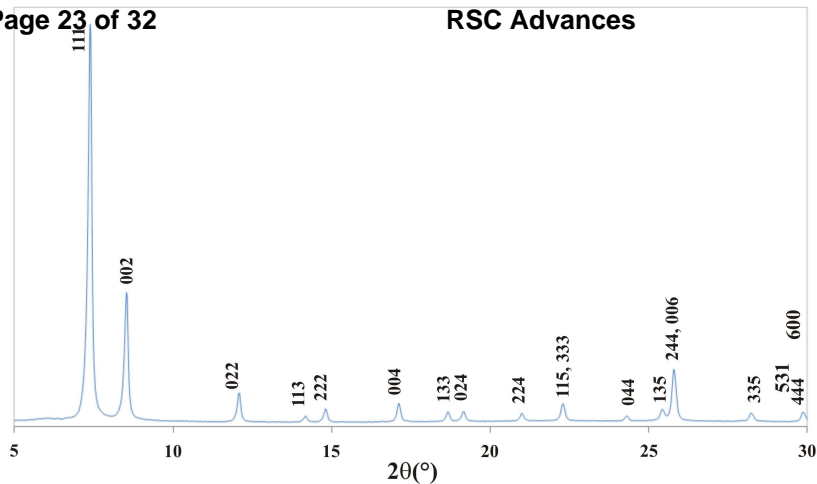
Figure 10: Schematic representation of the three precursor ligands. The energies of bounds ( $E_b$ ) and the resonance energies ( $E_r$ ) are provided to discuss the different possible destabilization mechanisms involved.

## Bibliography

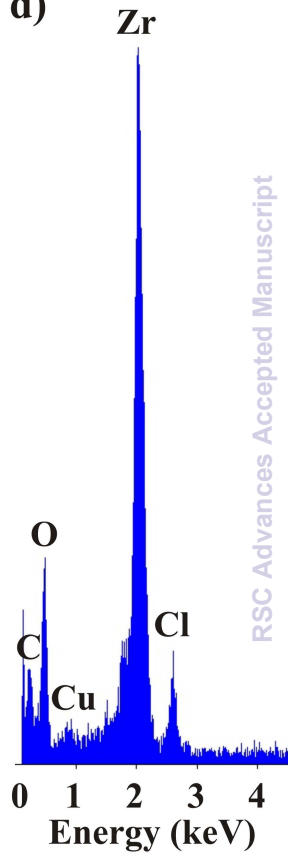
- [1] R. Bachelard, *Matériaux et techniques*, 1987, 75, 461.
- [2] F. K. Van Dijen, R. Metselaar, C. A. M. Siskens, *Spreksaal*, 1984, 117, 627.
- [3] E. G. Acheson, in *Carborundum; its history, manufacture and uses*, Philadelphia, 1893.
- [4]: Z. Dong, X Zhang, Q. Huang, J. Zhang, X. Zuo, W. Li, G. Yuan, X. Li, *Ceramics International*, 2015, 4 [6], 7359–7365
- [5]: C.L. Yan, R.J. Liu, Y. B. Cao, C.R. Zhang, D.K. Zhang, *Ceramics International*, 2013, 39, 3409–3412.
- [6] N. Scales, J. Chen, T. L. Hanley, D. P. Riley, G. R. Lumpkin and V. Luca, *Microporous and Mesoporous Materials*, 2015, 212, 100.
- [7]: M.D. Sacks, C.A. Wang, Z.H. Yang, A. Jain, *J. Mater. Sci.*, 2004, 39, 6057–6066.
- [8]: B. Cochepin, V. Gauthier, D. Vrel, *J. Cryst. Growth*, 2007, 304, 481–486.
- [9]: M. Song, M. Ran, Y. Long, *Journal of Alloys and Compounds*, 2013, 564, 20–26.
- [10] J. David, PhD thesis (in French), University of Limoges, n°25-2013, 2013
- [11] A. Maître, D. Tétard, P. Lefort, *J. Europ. Ceram. Soc.*, 2000, 20(1), 15.
- [12] M. D. Sacks, C.-A. Wang, Z. Yang, A. Jain, *Journal of Materials Science*, 2004, 39, 6057.
- [13] Y. Yan, Z. Huang, X. Liu, D. Jiang, *Journal of Sol-Gel Science and Technology*, 2007, 44, 81.
- [14] V. G. Sevastyanov, E. P. Simonenko, N. A. Ignatov, Y. S. Ezhov, N. P. Simonenko, N. T. Kuznetsov, *Russian Journal of Inorganic Chemistry*, 2011, 56, 661.
- [15] J. Hafizovic Cavka, S. Jakobsen, U. Olsbye, N. Guillou, C. Lamberti, S. Bordiga, K.P. Lillerud, *J. Am. Chem. Soc.*, 2008, 130, 13850-1.
- [16] S. Chavan, J.G. Vitillo, D. Gianolio, O. Zavorotynska, B. Civalieri, S. Jakobsen, M.H. Nilsen, L. Valenzano, C. Lamberti, K.P. Lillerud, S. Bordiga, *Phys. Chem. Phys.*, 2012, 14, 1614-26.
- [17] H.R. Abid, H. Tian, H.-M. Ang, M.O. Tade, C.E. Buckley, S. Wang, *Chem. Eng. J.*, 2012, 187 415-20.
- [18] Q. Yang, V. Guillermin, F. Ragon, A.D. Wiersum, P.L. Llewellyn, C. Zhong, T. Devic, G. Maurin, *Chem. Commun.*, 2012, 48, 9831-3.
- [19] C.H. Lau, R. Babarao, M.R. Hill, *Chem. Commun.*, 2013, 49, 3634-6.
- [20] S. Biswas, P. van der Voort, *Eur. J. Inorg. Chem.*, 2013, 2154-60.
- [21] H. Wu, Y.S. Chua, V. Krungleviciute, M. Tyagi, P. Chen, T. Yildirim, W. Zhou, *J. Am. Chem. Soc.*, 2013, 135, 10525-32.
- [22] P. Xydias, I. Spanopoulos, E. Klontzas, G.E. Froudakis, P.N. Trikalitis, *Inorg. Chem.*, 2014, 53, 679-81.

- [23] L. Li, S. Tang, C. Wang, X. Lv, M. Jiang, H. Wu, X. Zhao, *Chem. Commun.*, 2014, 50 2304-7.
- [24] N.H. Lee, D.W. Lee, H. Yeo, K. Kwak, H.S. Chun, K.M. Ok, *Cryst. Eng. Comm.*, 2014, 16, 5619-26.
- [25] B. Wang, H. Huang, X.-L. Lv, Y. Xie, M. Li, J.-R. Li, *Inorg. Chem.*, 2014, 53, 9254-59.
- [26] S. Biswas, J. Zhang, Z. Li, Y.-Y. Liu, M. Grzywa, L. Sun, D. Volkmer, P. van der Voort, *Dalton Trans.*, 2013, 42 4730-37.
- [27] B. Bozbiyik, T. Duerinck, J. Lannoeye, D.E. de Vos, G.V. Baron, *Mic. Mes. Mater.*, 2014, 183, 143-149.
- [28] P.S. Barcia, D. Guimaraes, P.A.P. Mendes, J.A.C. Silva, V. Guillerm, H. Chevreau, C. Serre, A. Rodrigues, *Mic. Mes. Mater.*, 2011, 139, 67.
- [29] Y. Luan, N. Zheng, Y. Qi, J. Yu, G. Wang, *Eur. J. Inorg. Chem.*, 2014, 4268-72.
- [30] B. Liu, H. Shioyama, T. Akita, Q. Xu, *J. Am. Chem. Soc.*, 2008, 130, 5390-1.
- [31] B. Liu, H. Shioyama, H. Jiang, X. Zhang, Q. Xu, *Carbon*, 2010, 48, 456-63.
- [32] W. Chaikittisilp, M. Hu, H. Wang, H.-S. Huang, T. Fujita, K.C.-W. Wu, L.-L. Chen, Y. Yamauchi, K. Ariga, *Chem. Commun.*, 2012, 48, 7259-61.
- [33] S. Lim, K. Suh, Y. Kim, M. Yoon, H. Park, D.N. Dybtsev, K. Kim, *Chem. Commun.*, 2012, 48, 7747-49.
- [34] S.J. Yang, T. Kim, J.H. Im, Y.S. Kim, K. Lee, H. Jung, C.R. Park, *Chem. Mater.*, 2012, 24 464-70.
- [35] K. Xi, S. Cao, X. Peng, C. Ducati, R.V. Kumar, A.K. Cheetham, *Chem. Commun.*, 2013, 49 2192-4.
- [36] L. Radhakrishnan, J. Reboul, S. Furukawa, P. Srinivasu, S. Kitagawa, Y. Yamauchi, *Chem. Mater.*, 2011, 23, 1225-31.
- [37] M. Gendre, A. Maître, G. Trolliard, *J. Europ. Ceram. Soc.*, 2011, 31, 2377-2385.
- [38] W. Zhang, H. Huang, D. Liu, Q. Yang, Y. Xiao, Q. Ma, C. Zhong, *Mic. Mes. Mater.*, 2013, 171 118-24.
- [39] V. Guillerm, S. Gross, C. Serre, T. Devic, M. Bauer, G. Férey, *Chem. Commun.*, 2010, 46, 767-9.
- [40] A. Schaate, P. Roy, A. Godt, J. Lippke, F. Waltz, M. Wiebke, P. Behrens, *Chem. Eur. J.*, 2011, 17, 6643-51.
- [41] G. Wißmann, A. Schaate, S. Lilienthal, I. Bremer, A. M. Schneider, P. Behrens, *Mic. Mes. Mater.*, 2012, 152, 64.
- [42] O. Masson, Peakoc profile fitting program, 2008,  
<http://www.esrf.eu/UsersAndScience/Experiments/TBS/SciSoft/OurSoftware/PEAKOC>.
- [43] J. David, G. Trolliard, M. Gendre, A. Maître, *J. Europ. Ceram. Soc.*, 2013, 33(1), 165.
- [44] J. David, G. Trolliard, C. Volkringer, Thierry Loiseau, O. Masson and Alexandre Maître, submitted to RSC-Advances.

Counts (a.u.)

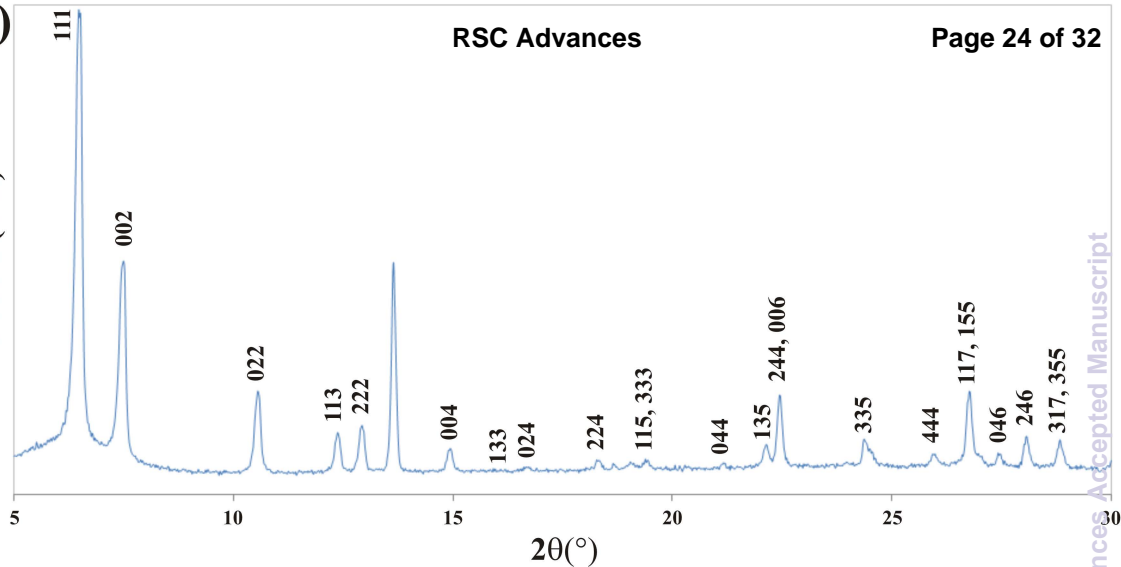
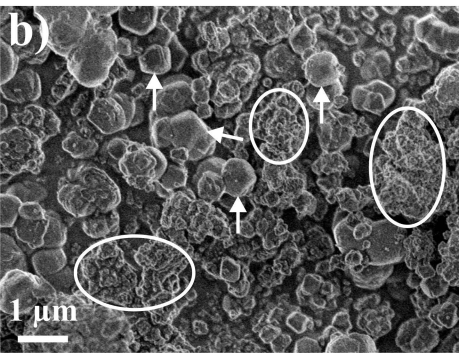
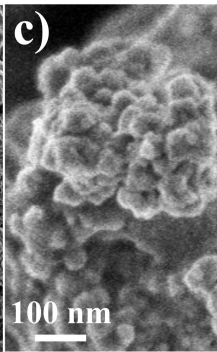
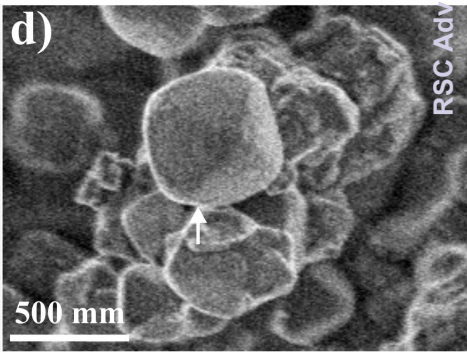


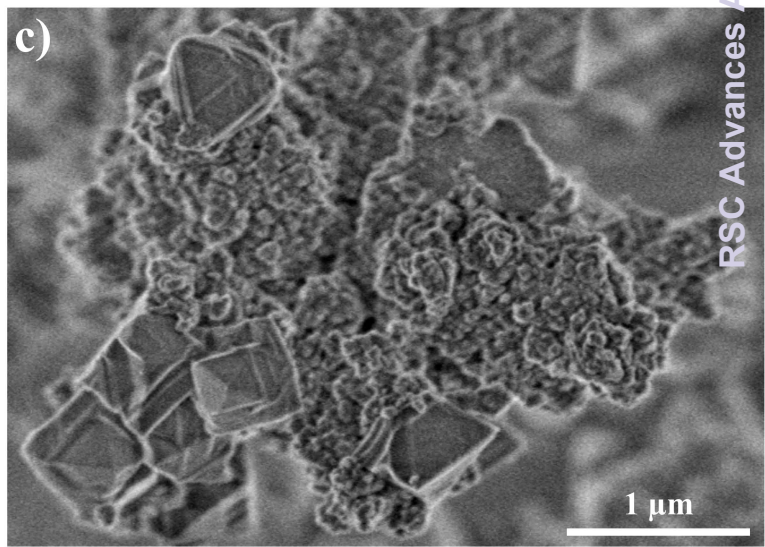
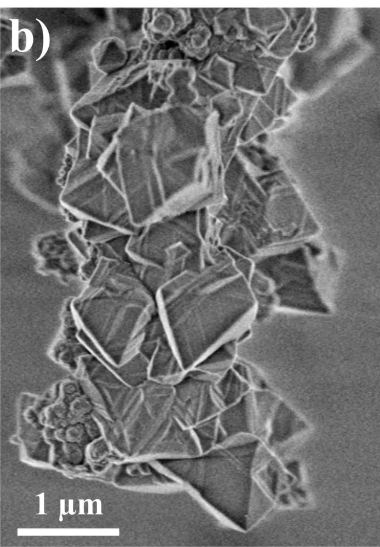
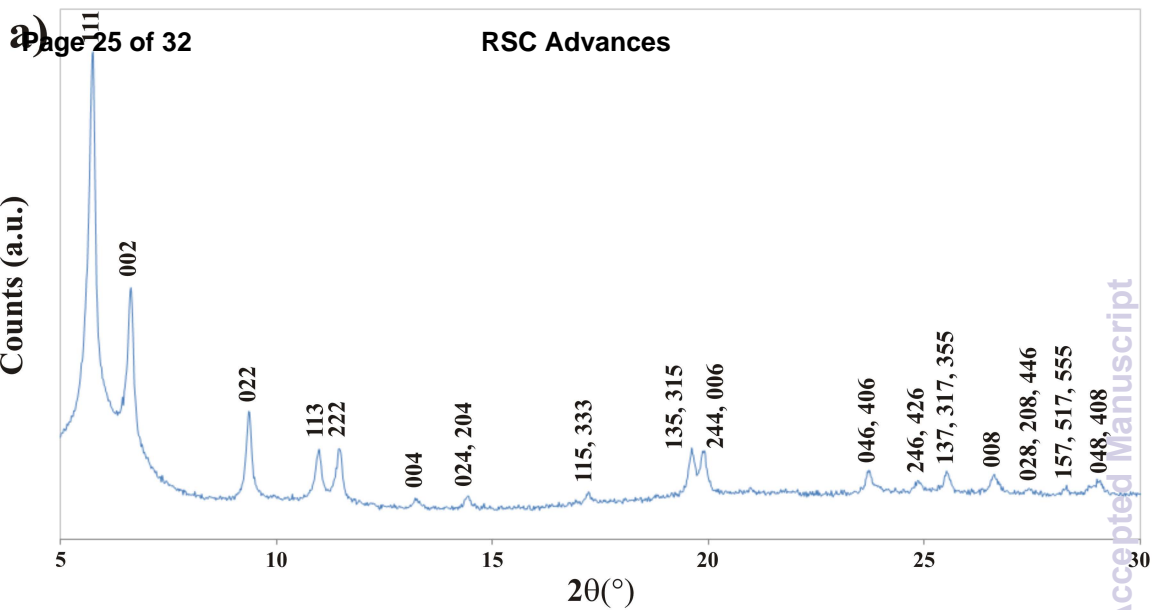
d)

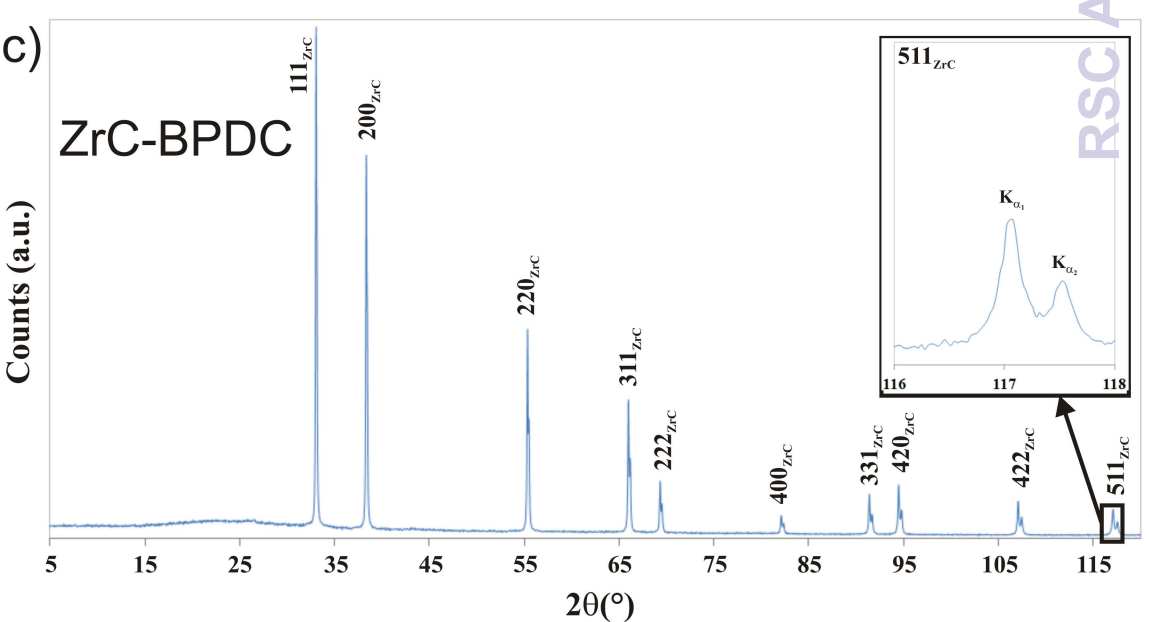
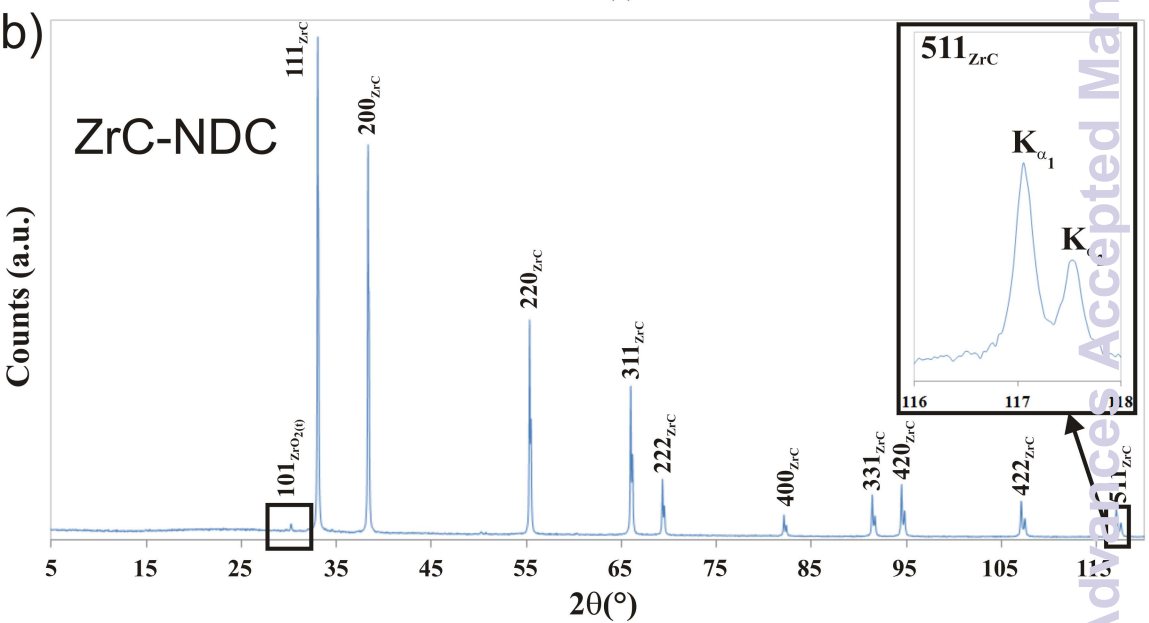
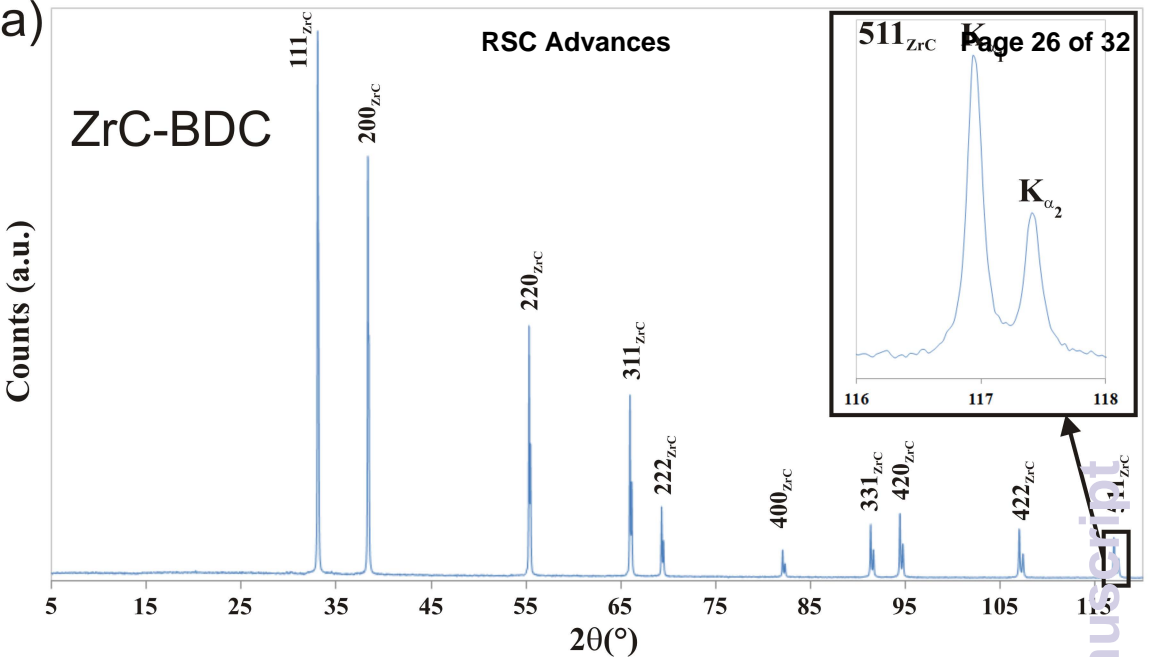


**a)**

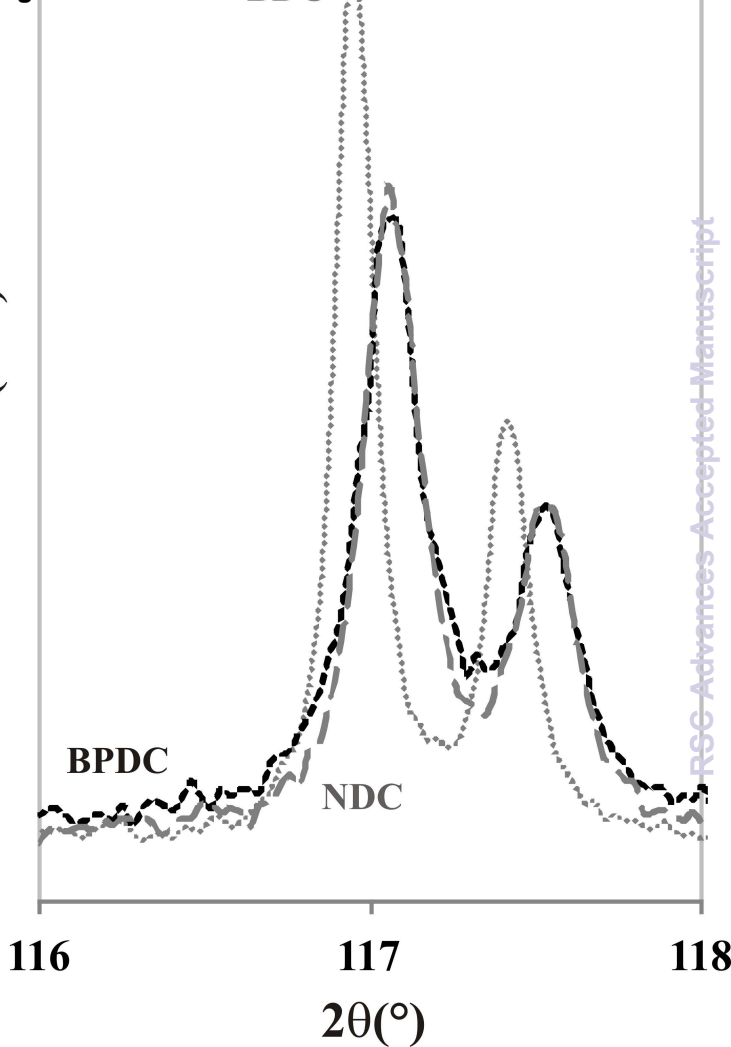
Counts (a.u.)

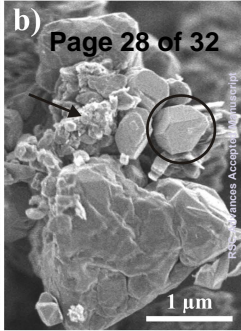
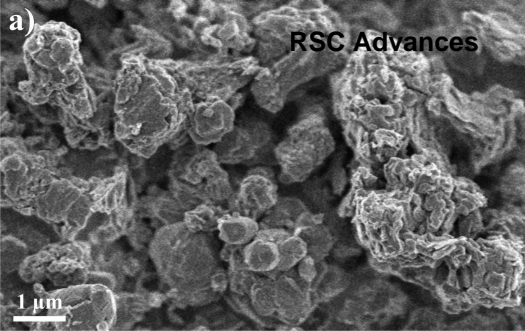
**b)****c)****d)**

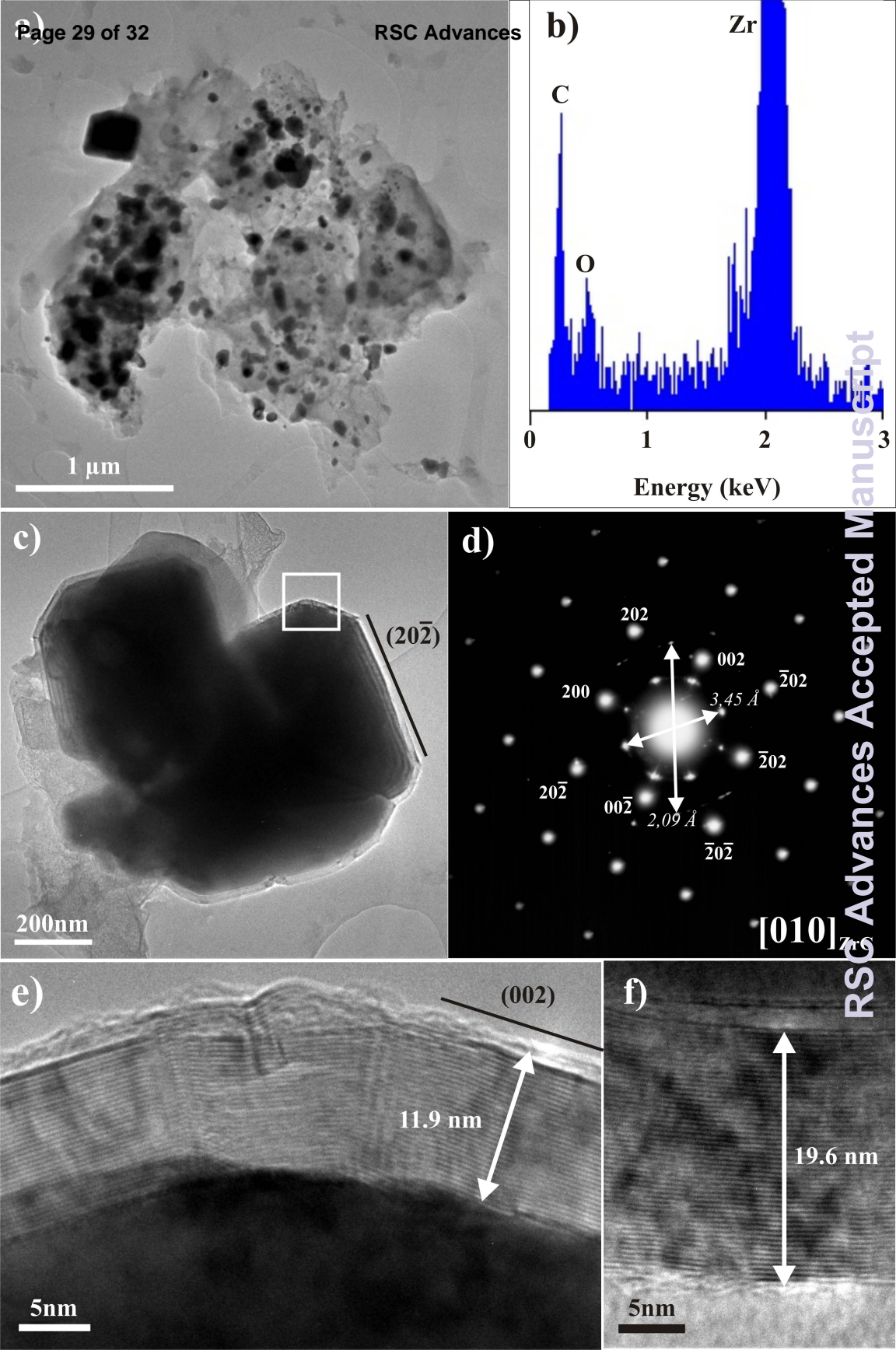


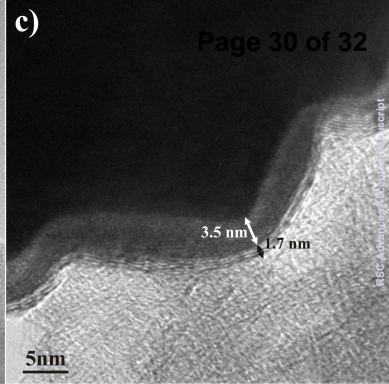
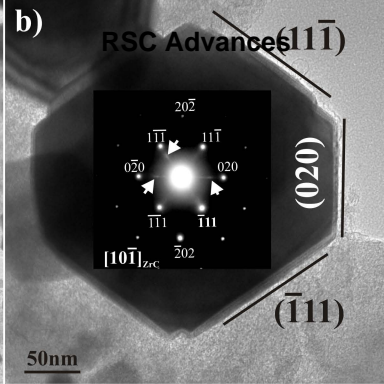
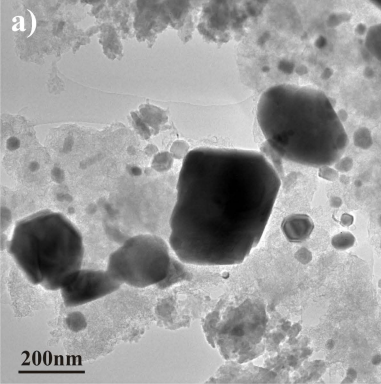


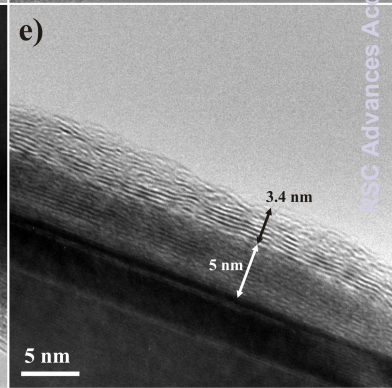
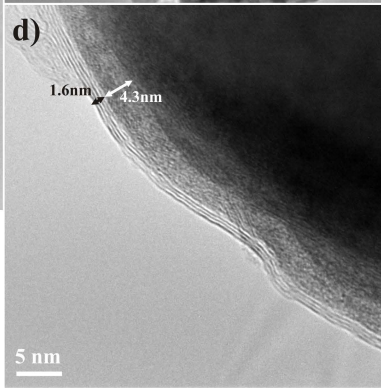
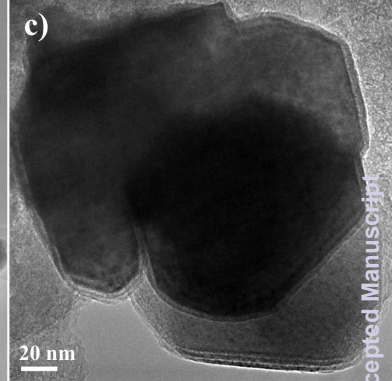
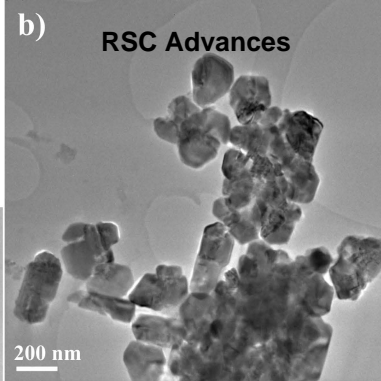
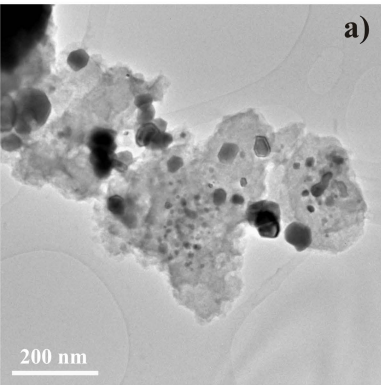
Counts (a.u.)



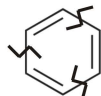
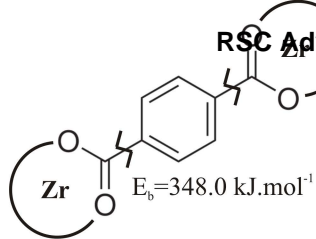






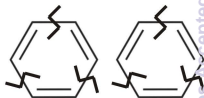
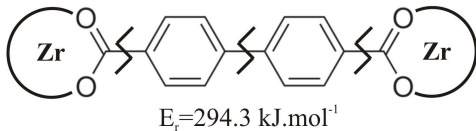


a) BDC

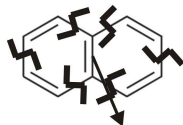
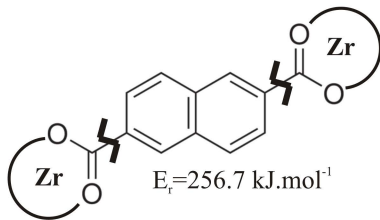


$$E_r = 150.9 \text{ kJ.mol}^{-1}$$

b) BPDC



c) NDC



$$E_b = 602.0 \text{ kJ.mol}^{-1}$$